Sensors and Materials, Vol. 38, No. 2 (2026) 639–652
MYU Tokyo

S & M 4333

Optical Properties and Energy Transfer Mechanism in Ce-doped P_2O_5–Al_2O_3–Cs_2O–Gd_2O_3 Glass Scintillators

Chie Morita,* Yutaka Fujimoto, Hiroki Kawamoto, and Keisuke Asai

Department of Applied Chemistry, Graduate School of Engineering, Tohoku University,
6-6-07, Aoba, Aramaki, Aoba-Ku, Sendai, Miyagi 980-8579, Japan

(Received October 22, 2025; accepted December 12, 2025)

Keywords: scintillator, Ce-doped glass, scintillation, photoluminescence

Inorganic glasses are promising candidates for scintillators because of their compositional flexibility, low cost, and ease of fabrication. However, their relatively low light yields and densities compared with those of crystal scintillators have limited their practical use, particularly for X-ray and γ-ray detection. In this study, P_2O_5–Al_2O_3–Cs_2O–Gd_2O_3–Ce_2O_3 glasses were prepared by the melt-quenching method under reduced pressure, aiming to enhance both light yield and effective atomic number (Z_{eff}). Ce^{3+} ions act as luminescent centers, whereas Gd^{3+} ions facilitate energy transfer and increase Z_{eff}. Structural, photoluminescence (PL), and scintillation properties were investigated for glasses with various Ce/Gd molar ratios. Under X-ray excitation, the synthesized glasses exhibited a broad emission band centered at approximately 350 nm, attributed to the 5d–4f transition ($^2F_{7/2,\ 5/2}$) of Ce^{3+} ions. The highest light yield reached 2100 photons/MeV under ^{137}Cs-γ-ray irradiation. The PL and scintillation decay profiles, as well as the temperature dependence of the emission spectra, indicate effective energy transfer from Gd^{3+} to Ce^{3+} ions. These results demonstrate that Ce^{3+}/Gd^{3+} co-doped phosphate glasses are promising materials for efficient glass scintillators applicable to X-ray and γ-ray detection.

1. Introduction

Glass materials are indispensable in a wide range of fields, including construction, medical devices, electronics, and optics, owing to their compositional flexibility, low cost, and ease of fabrication.[1,2] This intrinsic versatility enables fine-tuning of their physical and chemical properties and has stimulated increasing interest in using glass as a scintillator material for radiation detection.[3] Scintillators are phosphors that promptly convert the energy of ionizing radiation into low-energy photons, thereby enabling detection and analysis.[4] They play crucial roles in medical imaging,[5,6] security screening,[7] resource exploration,[8] and high-energy physics.[9–11] The performance of scintillation detectors critically depends on their material properties, and novel scintillators with improved performance are being actively developed. For X-ray and γ-ray detection, scintillators should exhibit high light yield for superior energy resolution, short decay times to minimize dead time, and a high effective atomic number (Z_{eff}) to

*Corresponding author: e-mail: morita.chie.r5@dc.tohoku.ac.jp
https://doi.org/10.18494/SAM6022

ISSN 0914-4935
https://myukk.org/

ensure high detection efficiency. Although most commercial scintillators are single crystals, glass scintillators are relatively uncommon despite their advantages of cost-effectiveness and compositional tunability. Among the few glass scintillators that have been commercialized, Ce-doped lithium silicate glass (e.g., GS20) is mainly used for thermal neutron detection.[12] In contrast, commercially available glass scintillators specifically designed for X-ray and γ-ray detection are still extremely limited because of their substantially lower light yield and density than those of conventional inorganic crystal scintillators. A variety of inorganic glass scintillators have been investigated using host matrices such as aluminoborate, aluminosilicate, silicate, phosphate, phosphosilicate, fluoride, and chloride glasses doped with emission centers such as Ce^{3+}, Eu^{2+}, and Tl^{+} ions. For example, Ce-doped SrF_2–Al_2O_3–B_2O_3 (240 photons/MeV),[13] Ce-doped Al_2O_3–B_2O_3–Gd_2O_3 (600 photons/MeV),[14] Ce-doped BaO–SiO_2–P_2O_5 (685 photons/MeV),[15] Ce-doped SrO–P_2O_5–Al_2O_3–Gd_2O_3 (1700 photons/MeV),[16] Ce-doped P_2O_5–Al_2O_3–Cs_2O (2500 photons/MeV),[17] Eu-doped SiO_2 (407 photons/MeV),[18] and Tl-doped SiO_2 (1100 photons/MeV)[19] have been reported as potential candidates. Among these, Ce-doped phosphate glasses containing Al and Cs exhibit particularly high light yields under ^{137}Cs γ-ray irradiation. Notably, these glass systems can incorporate relatively high Ce concentrations (≈ 10.7–13.8 mol%; Z_{eff} ≈ 43) without concentration quenching.[17,20–22] On the basis of these results, Ce-doped phosphate glass is considered a promising candidate for X-ray and γ-ray detection scintillators. In this study, phosphate-based glasses doped with Ce^{3+} ions as luminescent centers and Gd^{3+} ions as sensitizers were developed to achieve a high-light-yield glass scintillator for X-ray and γ-ray detection. The glass system P_2O_5–Al_2O_3–Cs_2O–Gd_2O_3–Ce_2O_3 was synthesized by the melt-quenching method under reduced pressure. P_2O_5 was selected as the host matrix because of its low melting point, high thermal stability, excellent transparency in the UV–visible region, and high solubility for rare-earth ions. Al_2O_3 and Cs_2O were introduced to stabilize the glass network. In phosphate glass networks, aluminum incorporates into the structure as [AlO_4] tetrahedra along with [PO_4] units, thereby enhancing the network connectivity and stability.[23] The addition of alkali modifiers such as Cs^{+} disrupts P–O–P linkages and increases the concentration of nonbridging oxygens, which improves the structural stability of the glass.[24] Gd^{3+} ions were introduced not only to increase the Z_{eff} of the glass but also to serve as energy donors for Ce^{3+} ions. Energy absorbed by Gd^{3+} under high-energy irradiation is expected to be transferred nonradiatively to neighboring Ce^{3+} ions, enhancing the overall scintillation efficiency.[25,26] Ce^{3+} ions act as luminescent centers, exhibiting fast 5d–4f transitions ($^2F_{7/2,\ 5/2}$) with decay times of approximately 30 ns and high light yield, as reported for similar glass systems.[20–22] In this work, the structural, photoluminescence (PL), and scintillation properties of P_2O_5–Al_2O_3–Cs_2O–Gd_2O_3–Ce_2O_3 glasses with varying Ce/Gd molar ratios were investigated, and the energy transfer mechanism between Ce^{3+} and Gd^{3+} ions was discussed.

2. Experimental Methods

2.1 Sample preparation

P_2O_5–Al_2O_3–Cs_2O–Gd_2O_3–Ce_2O_3 glasses were synthesized by the melt-quenching method under reduced pressure. Figure 1 shows an overview of the synthesis process. $Al(PO_3)_3$ (99%,

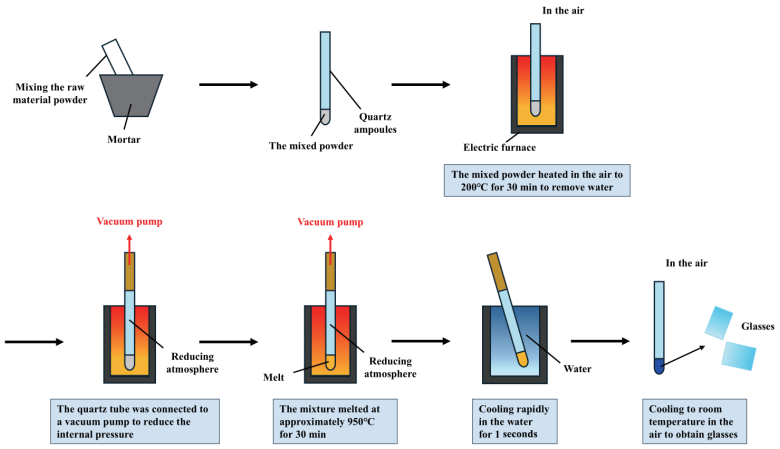

Fig. 1. (Color online) Schematic illustration of the glass synthesis process.

High Purity Chemicals), CsH_2PO_4 (99%, Mitsuwa Chemicals), $GdCl_3$ (99.9%, High Purity Chemicals), and $CeCl_3$ (99.99%, Sigma-Aldrich) were used as raw materials. The raw materials were mixed at the molar ratio of 1:1.5:(0.3−x):x (x = 0, 0.05, 0.10, and 0.15), corresponding to $Al(PO_3)_3$, CsH_2PO_4, $GdCl_3$, and $CeCl_3$, respectively. The mixed powders were placed in quartz ampoules and preheated in air at approximately 200 °C for 30 min in an electric furnace (FT-01P-150L, FULL-TECH) to remove moisture. Subsequently, the quartz ampoules were connected to a vacuum pump to reduce the internal pressure. This process was intended to prevent the oxidation of Ce^{3+} to Ce^{4+} by maintaining a reducing atmosphere. The materials inside the ampoules were then melted at approximately 950 °C for 30 min in the electric furnace, which is above the mixture's approximate melting point (≈ 900 °C). To cool the melt to below the glass transition temperature (T_g) and obtain an amorphous structure, the ampoules were quenched in water for approximately 1 s and then cooled to room temperature in air. Samples with dimensions of approximately 5–10 mm were selected and polished to achieve optically smooth surfaces for PL and scintillation measurements. Table 1 summarizes the raw-material-based and oxide-based compositions of the prepared glasses.

2.2 Measurement

The density of the glasses was measured by the Archimedes method using an electronic densimeter (DH-300, CgoldenWall JP). X-ray diffraction (XRD) patterns were recorded to confirm the amorphous nature of the samples using an X-ray diffractometer (Ultima IV-PXS, Rigaku) with Cu Kα radiation. The elemental composition of the glasses was determined by X-ray fluorescence (S8 TIGER 1 kW, Bruker), paying particular attention to halogen volatilization. Photoluminescence excitation (PLE) and emission spectra were measured using a spectrofluorometer (F-7000, Hitachi) equipped with a xenon lamp as the excitation source. The absolute PL quantum yields (PLQYs) were measured using a Quantaurus-QY system (C11347, Hamamatsu Photonics) with a 150 W Xe lamp. Each PLQY value represents the average of three measurements conducted under identical conditions. PL decay profiles were measured using a fluorescence lifetime spectrofluorometer (DeltaFlex 3000U-TMK2, Horiba). Light-emitting diodes with emission wavelengths of 255 nm (NanoLED-250, HORIBA Ltd.),

Table 1
Raw-material-based and oxide-based compositions of the prepared glasses.

Sample	Raw-material-based compositions	Oxide-based compositions
Undoped (x = 0)	$1Al(PO_3)_3$–$1.5CsPO_3$–$0.3GdCl_3$	$52P_2O_5$–$23Al_2O_3$–$17Cs_2O$–$7Gd_2O_3$
x = 0.05	$1Al(PO_3)_3$–$1.5CsPO_3$–$0.25GdCl_3$–$0.05CeCl_3$	$52P_2O_5$–$23Al_2O_3$–$17Cs_2O$–$5.8Gd_2O_3$–$1.2Ce_2O_3$
x = 0.10	$1Al(PO_3)_3$–$1.5CsPO_3$–$0.20GdCl_3$–$0.10CeCl_3$	$52P_2O_5$–$23Al_2O_3$–$17Cs_2O$–$4.7Gd_2O_3$–$2.3Ce_2O_3$
x = 0.15	$1Al(PO_3)_3$–$1.5CsPO_3$–$0.15GdCl_3$–$0.15CeCl_3$	$52P_2O_5$–$23Al_2O_3$–$17Cs_2O$–$3.5Gd_2O_3$–$3.5Ce_2O_3$

320 nm (NanoLED-320, HORIBA Ltd.), and 265 nm (SpectraLED-265, HORIBA Ltd.) were used as excitation sources. The pulse durations of NanoLED-250, NanoLED-320, and SpectraLED-265 were 1.2 ns, 1 ns, and 100 ns–1 ms, respectively. An optical cut-off filter was employed to remove scattered excitation light. To investigate the temperature dependence of the PL spectra, measurements were performed in the 10–300 K range using the same instrument as for the PL decay measurement, combined with a closed-type cryostat for temperature control. X-ray-induced radioluminescence (XRL) spectra were measured using a QE Pro spectrometer (Ocean Insight) coupled via an optical fiber. The sample was mounted at the fiber end, which was positioned at the irradiation port of the X-ray generator (XGD2300-HK, Rigaku) equipped with a Cu target operated at 40 kV and 4.0 mA. Temperature-dependent XRL spectra were recorded in the 10–300 K range using the same XRL system with a closed-cycle cryostat. Pulse-height spectra were measured and compared with the $Bi_4Ge_3O_{12}$ (BGO) reference sample (8600 photons/MeV)[27] to estimate the scintillation light yield. The spectra were obtained using a photomultiplier tube (PMT; R7600-200, Hamamatsu Photonics) and 662 keV γ-rays from a ^{137}Cs source. The sample was optically coupled to the PMT with optical grease (TSF 451-50 M, GE Toshiba) and wrapped in Teflon tape as a reflector. Signals from the PMT were processed through a preamplifier (113, Ortec), a shaping amplifier (572, Ortec), and a multichannel analyzer (MCA; MCA8000D, Amptek). The light yield of the glasses was estimated by comparing the channel number of the 662 keV γ-ray photoabsorption peak of the ^{137}Cs source with that of the BGO standard. Corrections were applied for the PMT quantum efficiency at the emission wavelength of each sample. Scintillation decay profiles were measured by the delayed coincidence method[28] using the original setup described in our previous report.[29] In this configuration, a ^{22}Na source emitting 511 keV γ-rays was used for excitation.

3. Results and Discussion

3.1 Structural and physical properties

Figure 2(a) shows photographs of the synthesized glasses with x = 0.05, 0.10, and 0.15 under visible light. All samples were transparent and showed no noticeable deliquescence. Figure 2(b) shows the XRD patterns of the synthesized glasses in the 2θ range of 5°–80°. All samples exhibited a broad halo without distinct diffraction peaks, confirming their amorphous nature.

Table 2 summarizes the densities and effective atomic numbers (Z_{eff}) of the glasses with various Ce (x) and Gd ($0.3-x$) molar ratios. The decreases in density and Z_{eff} with decreasing Gd concentration are attributed to the substitution of Gd (Z = 64) by Ce (Z = 58). This replacement

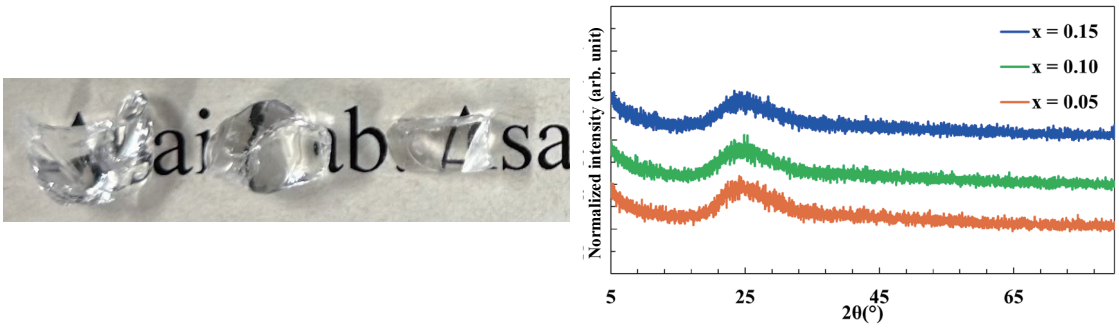

(a) (b)

Fig. 2. (Color online) (a) Photographs under visible light and (b) XRD patterns of the synthesized $Al(PO_3)_3$–$1.5CsPO_3$–$(0.3–x)GdCl_3$–$xCeCl_3$ glasses (x = 0.05, 0.10, and 0.15).

Table 2
Densities and effective atomic numbers (Z_{eff}) of the synthesized glasses (x = 0.05, 0.10, and 0.15).

Sample	Density (g/cm$_3$)	Z_{eff}
x = 0.05	3.19	44.9
x = 0.10	3.11	44.6
x = 0.15	3.05	44.4

lowers the average atomic number, leading to a reduction in Z_{eff}. Furthermore, since Gd has a higher atomic mass than Ce, decreasing the Gd content also reduces the overall density of the glass. The densities of the synthesized glasses (3.05–3.19 g/cm^3) are higher than that of GS20 (2.5 g/cm^3), the only glass scintillator currently in practical use for neutron measurement.[30] In addition, these values are comparable to those of previously reported glass scintillators[15,21,31] and the commercial NaI:Tl$^+$ crystal (3.67 g/cm^3).[32] The synthesized glasses also exhibit Z_{eff} (44.4–44.9) exceeding that of GS20 (≈ 24).[30] These values are comparable to those of heavy-element-containing glass scintillators[15] and to that of $CeBr_3$ (≈ 47).[33] Because the present glasses possess densities and effective atomic numbers comparable to those of commercial scintillators such as NaI:Tl$^+$ and $CeBr_3$, they are expected to be promising candidates for γ-ray detection, provided that a scalable and reproducible fabrication process can be established. Table 3 presents the elemental compositions of the synthesized glasses, as determined by XRF analysis. The compositions of $Al(PO_3)_3$ and $CsPO_3$ were calculated from the elemental concentrations obtained by XRF, assuming complete oxidation. Notably, the fabricated glasses were nearly free of chlorine (Cl), which is attributed to Cl volatilization under high-temperature and reduced-pressure conditions during melting under vacuum.

3.2 PL properties

Figure 3(a) shows the PLE spectra monitored at 310 nm and the PL spectra monitored at 220 and 270 nm for undoped $Al(PO_3)_3$–$1.5CsPO_3$–$0.3GdCl_3$ glass. The PLE spectra exhibit excitation bands in the 220–250 nm range and at approximately 270 nm, corresponding to the optical transitions from $^8S_{7/2}$ to $^6D_{1/2,\ 9/2}$ and from $^8S_{7/2}$ to ^6I_J of Gd^{3+} ions.[26,34,35] Upon excitation at 220 and 270 nm, a distinct emission peak at approximately 310 nm was observed, which is attributed to the $^6P_{7/2} \rightarrow {}^8S_{7/2}$ transition of Gd^{3+} ions[34,36] Figure 3(b) presents the PLE and PL

Table 3
Elemental compositions of the synthesized glasses (x = 0, 0.05, 0.10, and 0.15).

Sample	Element composition (wt%)				
	Cl	Ce	Gd	$Al(PO_3)_3$	$CsPO_3$
Undoped	0.033	N/A	7.096	39.502	53.061
x = 0.05	0.008	0.928	6.037	39.313	52.911
x = 0.10	0.020	1.985	4.726	39.279	53.664
x = 0.15	0.026	3.235	3.593	39.134	53.578

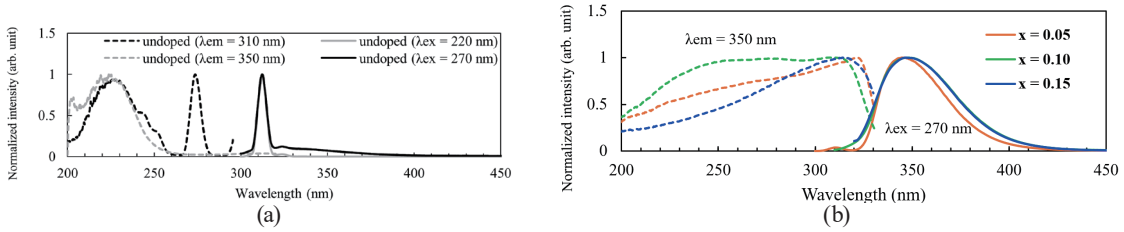

Fig. 3. (Color online) (a) PLE (λ_{em} = 310 nm) and PL (λ_{ex} = 220 and 270 nm) spectra of the undoped $Al(PO_3)_3$–$1.5CsPO_3$–$0.3GdCl_3$ glass. (b) PLE (λ_{em} = 350 nm) and PL (λ_{ex} = 270 nm) spectra of the synthesized $Al(PO_3)_3$–$1.5CsPO_3$–$(0.3-x)GdCl_3$–$xCeCl_3$ glasses (x = 0.05, 0.10, and 0.15).

spectra of the Ce-doped $Al(PO_3)_3$–$1.5CsPO_3$–$(0.3-x)GdCl_3$–$xCeCl_3$ glasses with x = 0.05, 0.10, and 0.15. The glasses exhibit a broad excitation band between 220 and 320 nm, assigned to the 4f ($^2F_{5/2,\ 7/2}$) → 5d transition of Ce^{3+} ions. PL spectra were recorded under 270 nm excitation, which corresponds to the $^8S_{7/2} \rightarrow {}^6I_J$ transition region of Gd^{3+} ions. The Ce-doped glasses show a broad emission band centered at around 350 nm, attributed to the 5d → 4f transition ($^2F_{7/2,\ 5/2}$), the characteristic of Ce^{3+} emission.[22,26,37,38] Notably, the 310 nm emission from Gd^{3+} ions observed in the undoped glass disappeared in the Ce-doped samples. This phenomenon has been reported in various Ce/Gd-co-doped glasses and crystals.[26,36,39–41] Figures 3(a) and 3(b) also reveal the overlap between the Gd^{3+} emission and Ce^{3+} excitation bands, indicating the presence of energy transfer from Gd^{3+} to Ce^{3+} ions (Förster mechanism) or reabsorption.

Figure 4(a) shows the PLQYs of the synthesized glasses (x = 0.05, 0.10, and 0.15) under 290 nm. The PLQYs reached maximum at an excitation wavelength of 290 nm. In addition, they remained almost constant within the 290–310 nm excitation range, with a fluctuation of less than ±5%. The average PLQYs were 84.5, 84.9, and 90%, respectively. These high values are comparable to those of previously reported Ce^{3+}-doped glass scintillators with high light yields, such as $Al(PO_3)_3$–$CsPO_3$–$CeBr_3$ glass (91.5%),[17] $Al(PO_3)_3$–$CsPO_3$–$CsBr$–$CeBr_3$ glass (92.7%),[42] and Ce-doped MgF_2–Al_2O_3–B_2O_3 glass (80–100%).[43] Even at the high Ce^{3+} concentration of 5.4 mol% (x = 0.15), no concentration quenching was observed, and the high quantum yields were maintained. These results indicate that this glass effectively suppresses quenching processes, including concentration quenching due to the aggregation of luminescent centers,[44] thermal quenching,[45,46] and energy transfer to Ce^{4+} ions.[47] Figures 4(b) and 4(c) present the PL decay profiles of the undoped and Ce-doped glasses (x = 0.05, 0.10, and 0.15). To identify whether energy transfer or reabsorption occurs, the PL decay profiles for the 310 nm emission of Gd^{3+} were recorded under 265 nm excitation with varying Ce concentrations. For the undoped glass, the decay curve was well fitted by a single-exponential function, giving a decay constant τ of 5.66 ms, consistent with the $^6P_{7/2} \rightarrow {}^8S_{7/2}$ transition of Gd^{3+} ions.[40] In the Ce-

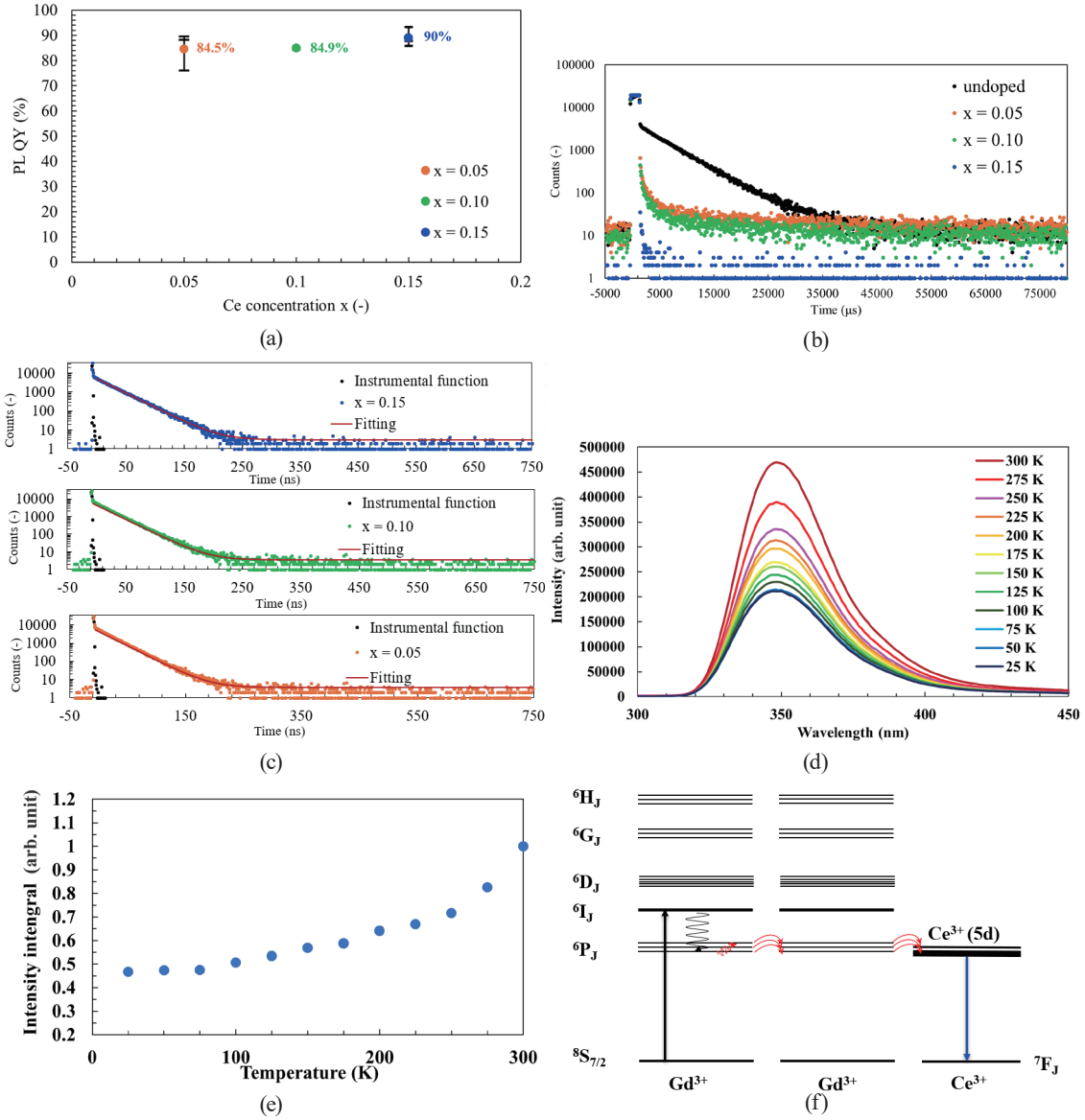

Fig. 4. (Color online) (a) PLQYs of the synthesized $Al(PO_3)_3$–$1.5CsPO_3$–$(0.3–x)GdCl_3$–$xCeCl_3$ glasses (x = 0.05, 0.10, and 0.15) under 290 nm excitation, (b) PL decay profiles of the synthesized $Al(PO_3)_3$–$1.5CsPO_3$–$(0.3–x)GdCl_3$–$xCeCl_3$ glasses (x = 0.05, 0.10, and 0.15) recorded under 265 nm excitation and 310 nm emission, (c) PL decay profiles of the synthesized $Al(PO_3)_3$–$1.5CsPO_3$–$(0.3–x)GdCl_3$–$xCeCl_3$ glasses (x = 0.05, 0.10, and 0.15) recorded under 320 nm excitation and 350 nm emission, (d) temperature dependence of the PL emission spectra of the synthesized $Al(PO_3)_3$–$1.5CsPO_3$–$(0.3–x)GdCl_3$–$xCeCl_3$ glass (x = 0.15) upon excitation of Gd^{3+} ions at 255 nm, (e) temperature dependence of the integrated intensity of the PL emission spectra of the same glass under excitation of Gd^{3+} ions at 255 nm, and (f) schematic illustration of the Gd^{3+}–Gd^{3+} energy migration and Gd^{3+}–Ce^{3+} energy-transfer mechanisms in the synthesized glass.

doped samples, the decay profiles were fitted by a double-exponential function, revealing two components: a slow one (τ_1 = 3.1–2.2 ms) and a fast one (τ_2 = 0.225–0.200 ms), as summarized in Table 4. The slow component (τ_1) can be attributed to the 4f–4f transition of Gd^{3+} ions. With increasing Ce concentration, the Gd^{3+} luminescence decayed more rapidly, confirming

Table 4
Estimated PL decay constants of the synthesized glasses under 265 nm excitation and monitoring Gd^{3+} emission at 310 nm.

Sample	PL decay constant	
	τ_1 (ms)	τ_2 (ms)
Undoped	5.66	N/A
$x = 0.05$	3.10	0.207
$x = 0.10$	3.05	0.225
$x = 0.15$	2.23	0.200

quenching. This behavior is attributed to energy transfer from Gd^{3+} to Ce^{3+} ions, consistent with the disappearance of Gd^{3+} emission and the spectral overlap between the Gd^{3+} emission and Ce^{3+} excitation bands. Such mechanisms have been reported in Ce^{3+}-doped GdP_3O_9 metaphosphate,[40] $Gd_2(SiO_4)O:Ce$,[41] Ce^{3+}-doped phosphate glasses,[26] and Ce^{3+}-doped gadolinium oxyfluoroborate glasses.[36] In the Ce-doped glasses, a resonance energy transfer from Gd^{3+} to Ce^{3+} is expected to occur. Therefore, the fast component (τ_2) is likely associated with the $Gd^{3+} \rightarrow Ce^{3+}$ energy transfer. This interpretation is consistent with the rapid decay of Gd^{3+} luminescence observed with increasing Ce concentration. Figure 4(c) shows the PL decay profiles of the Ce^{3+} emission at 350 nm under 320 nm excitation for the glasses with $x = 0.05$, 0.10, and 0.15. The initial rapid decay observed immediately after excitation is attributed to the instrument response function. All decay curves were well fitted by a single-exponential function, giving decay constants τ = 27–29 ns (Table 5). The decay times remained nearly constant irrespective of Ce concentration, indicating negligible concentration quenching, consistent with the PLQY results. These lifetimes agree with previously reported values for Ce-doped phosphate glasses[22,48] and correspond to the 5d → 4f transition ($^2F_{7/2,\ 5/2}$) of Ce^{3+} ions. Figure 4(d) shows the PL spectra of the $x = 0.15$ glass under 255 nm excitation in the Gd^{3+} absorption region at 25–300 K. A broad Ce^{3+} emission band peaking at ≈ 350 nm was observed at all temperatures. As the temperature increased to 300 K, the integrated PL intensity gradually increased without evidence of thermal quenching [Fig. 4(e)]. This enhancement is attributed to the phonon-assisted population of higher-energy Gd^{3+} excited states, particularly $^6P_{5/2}$, which promotes energy migration among Gd^{3+} ions through increased overlap between Gd^{3+} emission and Ce^{3+} excitation bands, thereby enhancing $Gd^{3+} \rightarrow Ce^{3+}$ energy transfer. These observations are consistent with previous reports that phonon-assisted processes play a crucial role in Gd^{3+}/Ce^{3+} co-doped systems.[40] A schematic illustration of the Gd^{3+}–Gd^{3+} and Gd^{3+}–Ce^{3+} energy-transfer mechanisms in the synthesized glasses is presented in Fig. 4(f).

3.3 Scintillation properties

Figure 5 shows the XRL spectra of the synthesized $Al(PO_3)_3$–$1.5CsPO_3$–$(0.3-x)GdCl_3$–$xCeCl_3$ glasses with $x = 0.05$, 0.10, and 0.15. The fabricated glasses exhibit broad emission bands in the 320–400 nm range with a maximum at 350 nm, which are attributed to the optical transition from the 5d lowest excited state to the 4f ($^2F_{7/2,\ 5/2}$) ground states of Ce^{3+} ions.[22,26,37,38] Notably, the emission peak wavelength and spectral shape of the synthesized glasses remain unchanged with varying Ce^{3+} concentrations. Furthermore, as in the PL spectra, no

Table 5
Estimated PL decay constants of the synthesized glasses under 320 nm excitation and monitoring Ce^{3+} emission at 350 nm.

Sample	PL decay constant
	τ (ns)
x = 0.05	27.3
x = 0.10	27.3
x = 0.15	28.6

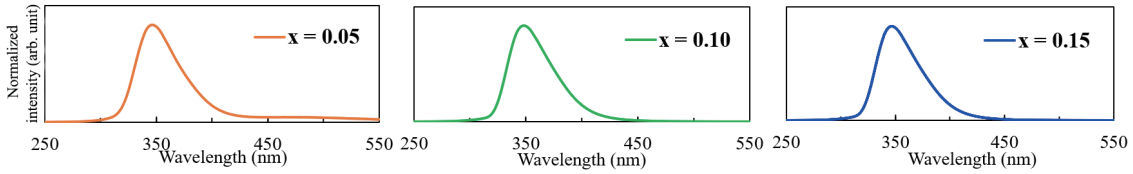

Fig. 5. (Color online) XRL spectra of the synthesized $Al(PO_3)_3$–$1.5CsPO_3$–$(0.3–x)GdCl_3$–$xCeCl_3$ glasses (x = 0.05, 0.10, and 0.15).

emission from Gd^{3+} ions was detected under X-ray excitation, indicating efficient energy transfer from Gd^{3+} to Ce^{3+} ions. The emission wavelength of Ce-doped borosilicate and silica glass systems is typically around 430 nm.[26,49] In contrast, the synthesized phosphate-based glasses developed in this study show an emission peak at approximately 350 nm, consistent with previously reported phosphate glass systems. This emission wavelength also falls within the optimal sensitivity range of PMTs, making the material well suited to scintillation applications. Figure 6(a) shows the XRL spectra of the x = 0.15 glass measured in the temperature range of 25–300 K. Broad Ce^{3+} emission bands peaking at 350 nm were observed at all temperatures. As shown in Fig. 6(b), the integrated intensity of the XRL spectra gradually increased with temperature up to 300 K, a trend consistent with the PL results. This temperature-dependent enhancement is attributed to the phonon-assisted population of higher-energy excited states of Gd^{3+} ions, particularly the $^6P_{5/2}$ level. Although the increase in XRL intensity is smaller (~25%) than that observed in the PL spectra, it remains significant. Under radiation excitation, additional energy transfer channels likely contribute to the temperature dependence, including Ce^{3+}–Ce^{3+} energy transfer,[50] transfer from self-trapped excitons (STEs) to Ce^{3+},[51,52] and transfer from trap sites to Ce^{3+},[53] in addition to the primary $Gd^{3+} \rightarrow Ce^{3+}$ transfer pathway. Figure 7 shows the scintillation decay profiles of the synthesized $Al(PO_3)_3$–$1.5CsPO_3$–$(0.3–x)GdCl_3$–$xCeCl_3$ glasses with x = 0.05, 0.10, and 0.15. The decay curves were fitted using a sum of three exponential components, and the estimated decay constants are summarized in Table 6. The initial fast component observed immediately after the rise is attributed to the instrumental response function (IRF). The first decay component (τ_1, faster component) ranged from 32 to 37 ns and corresponds to the 5d → 4f transition ($^2F_{7/2,\ 5/2}$) of Ce^{3+} ions.[22,48] Compared with the PL decay constants shown in Fig. 4(c), the scintillation decay constant τ_1 was slightly longer, which can be attributed to energy transfer from Gd^{3+} to Ce^{3+} ions. The second component (τ_2, slower component) ranged from 133 to 207 ns and is considered to originate from the relatively slow energy transfer from the glass host to Ce^{3+} ions, consistent with previous reports on Ce-doped glass scintillators.[20,22,54] Figure 8 presents the pulse-height spectra under ^{137}Cs γ-ray irradiation

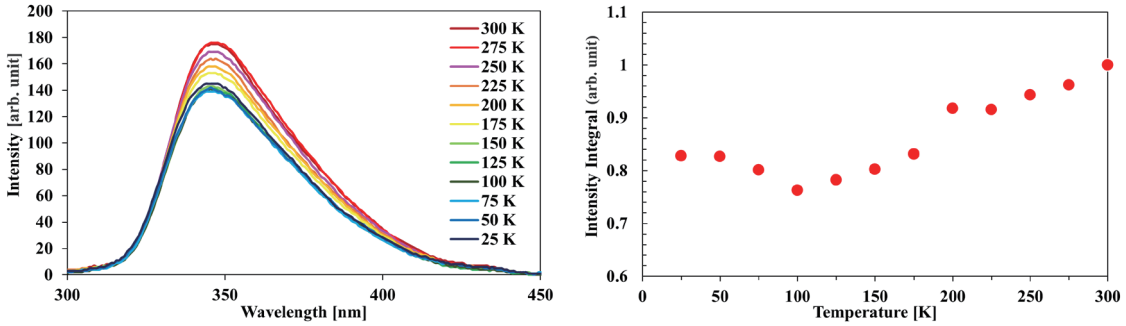

Fig. 6. (Color online) (a) Temperature dependence of the XRL spectra of the synthesized $Al(PO_3)_3$–$1.5CsPO_3$–$(0.3-x)GdCl_3$–$xCeCl_3$ glass ($x = 0.15$) and (b) temperature dependence of the integrated intensity of the XRL spectra of the same glass.

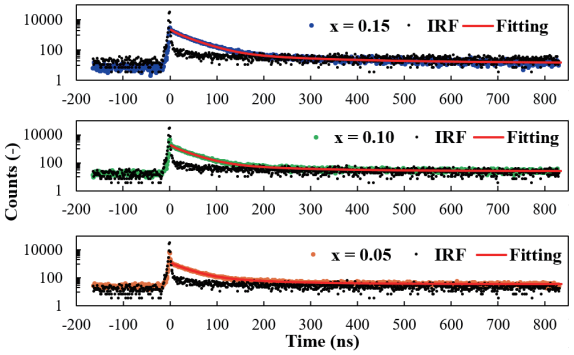

Fig. 7. (Color online) Scintillation decay profiles of the synthesized $Al(PO_3)_3$–$1.5CsPO_3$–$(0.3-x)GdCl_3$–$xCeCl_3$ glasses ($x = 0.05$, 0.10, and 0.15).

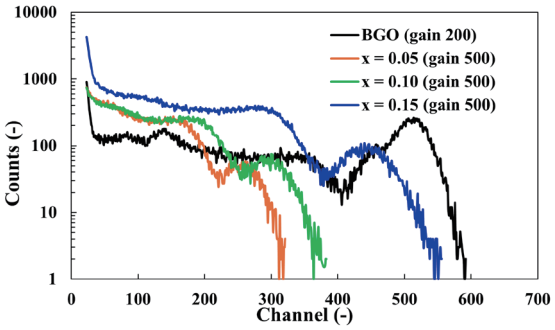

Fig. 8. (Color online) Pulse-height spectra under 137Cs γ-ray-irradiation for the synthesized $Al(PO_3)_3$–$1.5CsPO_3$–$(0.3-x)GdCl_3$–$xCeCl_3$ glasses ($x = 0.05$, 0.10, and 0.15) and the BGO reference.

Table 6
Estimated scintillation decay constants of the synthesized $Al(PO_3)_3$–$1.5CsPO_3$–$(0.3-x)GdCl_3$–$xCeCl_3$ glasses ($x = 0.05$, 0.10, and 0.15).

Sample	Scintillation decay constant		
	τ_1 (ms)	τ_2 (ms)	*IRF* (ns)
$x = 0.15$	37 (69%)	207 (2%)	9.6 (28%)
$x = 0.10$	33 (71%)	155 (4%)	6.3 (25%)
$x = 0.05$	32 (76%)	133 (7%)	4.27 (16%)

for the synthesized glasses and a BGO reference sample. All fabricated samples exhibited a photoelectric peak corresponding to the full-energy absorption of the 662 keV γ-ray from the ^{137}Cs source. The channel positions of these peaks were determined by fitting the peak profiles with a Gaussian function. The light yield for each sample was calculated using Eq. (1).

$$Light\,Yield_{sample} = Light\,Yield_{ref} \times \frac{Channel_{sample}}{Channel_{ref}} \times \frac{QE_{ref}}{QE_{sample}} \quad (1)$$

Here, "*Channel*" denotes the channel number of the photoabsorption peak for the 662 keV γ-ray, and "*QE*" represents the quantum efficiency of the photomultiplier tube used in the

Table 7
Light yields of various glass scintillators.

Sample	Light yield (photons/MeV)
$Al(PO_3)_3$–1.5$CsPO_3$–0.15$GdCl_3$–0.15$CeCl_3$ (this study)	2100
SiO_2–LiF–Al_2O_3–$GdBr_3$–$CeBr_3$	3200 (Ref. 56)
Ce-doped SiO_2–Al_2O_3–BaF_2–Gd_2O_3	2100 (Ref. 57)
Ce-doped BaF_2-Al_2O_3-B_2O_3	1800 (Ref. 58)
Ce-doped SrO–P_2O_5–Al_2O_3–Gd_2O_3	1700 (Ref. 59)
P_2O_5–Li_2O–GdI_3–Al_2O_3–Ca_2CO_3–$CeBr_3$	1600 (Ref. 26)
Ce-doped SiO_2–B_2O_3–Al_2O_3–Gd_2O_3	910 (Ref. 60)
Ce-doped Al_2O_3–B_2O_3–Gd_2O_3	600 (Ref. 14)

measurement. The samples with x = 0.05, 0.10, and 0.15 exhibited photoabsorption peaks at 252, 292, and 440 channels, respectively, while the BGO reference showed a peak at 1265 channels. The *QE* values were dependent on the emission peak wavelength of each material: the synthesized glasses exhibited a 350 nm emission peak with *QE* = 0.35, while the BGO emitted at 480 nm with a *QE* = 0.25. An increase in Ce concentration led to a corresponding increase in light yield, reaching 1200, 1400, and 2100 photons/MeV for x = 0.05, 0.10, and 0.15, respectively. An increase in Ce concentration led to a corresponding increase in light yield, reaching 1200, 1400, and 2100 photons/MeV for x = 0.05, 0.10, and 0.15, respectively. Although the PLQY remained nearly constant, the increase in light yield can be attributed to the enhanced overall energy transfer efficiency at higher Ce concentrations. In this concentration range, both the host-to-Ce and Gd–Ce energy transfer pathways become more efficient, thereby increasing the probability that the absorbed energy is ultimately released as radiative emission from Ce^{3+} ions. This trend is considered to originate from the comparable concentrations of Ce and Gd ions in the glass matrix, which facilitates efficient energy migration toward Ce^{3+}. In contrast, the energy resolutions of the synthesized glasses with x = 0.05, 0.10, and 0.15 were 26, 25, and 19%, respectively. Compared with previously developed Ce-doped phosphate glass scintillators—such as Ce-doped $Al(PO_3)_3$–$CsPO_3$ glass[17] and Ce-doped $Al(PO_3)_3$–$Sr(PO_3)_2$–$CsPO_3$ glass,[22] which demonstrated energy resolutions of approximately 15%—the glasses synthesized in this study exhibit significantly poorer resolution (26%). This degradation is likely due to the presence of an escape peak originating from the Gd Kα line (42.7 keV). Such escape events appear as low-energy shoulders or asymmetric tails in the spectra, broadening the photoabsorption peak and thus degrading the energy resolution.[55] Table 7 summarizes the light yields of various Ce-doped glass scintillators. Compared with previously reported glass scintillators, the light yield achieved in this study can be regarded as moderate.

4. Conclusions

P_2O_5–Al_2O_3–Cs_2O–Gd_2O_3–Ce_2O_3 glasses were successfully synthesized by the melt-quenching method under reduced pressure. PL and scintillation properties were investigated, with particular emphasis on the energy-transfer mechanism between Gd^{3+} and Ce^{3+} ions. The Ce-doped glasses exhibited a broad emission band centered at ~350 nm, attributed to the 5d → 4f transition ($^2F_{7/2,\ 5/2}$) of Ce^{3+} ions, whereas the ~310 nm Gd^{3+} emission observed in the undoped

glass was quenched upon Ce^{3+} incorporation. PL decay measurements further supported this mechanism, showing shortened Gd^{3+} decay times with increasing Ce^{3+} concentration, indicative of $Gd^{3+} \rightarrow Ce^{3+}$ energy transfer. Temperature-dependent PL and XRL spectra showed an increase in luminescence intensity with increasing temperature. This enhancement is attributed to the phonon-assisted population of higher ^6P excited states of Gd^{3+} ions, which improves spectral overlap with the Ce^{3+} excitation bands and facilitates more efficient energy transfer. The optimal composition was identified as $x = 0.15$ (Ce/Gd molar ratio = 1.0), yielding a maximum light yield of 2100 photons/MeV and an energy resolution of 19% under ^{137}Cs γ-ray irradiation. These results demonstrate the successful development of a highly luminescent phosphate-glass scintillator based on efficient $Gd^{3+} \rightarrow Ce^{3+}$ energy transfer. Overall, the P_2O_5–Al_2O_3–Cs_2O–Gd_2O_3–Ce_2O_3 system offers a promising pathway toward high-performance inorganic glass scintillators for X-ray and γ-ray detection.

Acknowledgments

This work was supported by Grant-in Aid for Scientific Research (A) (Grant No. 22H00308, 2022–2026), Grant-in-Aid for Challenging Research (Exploratory) (Grant No. 24K21544, 2024–2026), and Grant-in-Aid for Scientific Research (B) (Grant No. 25K01702, 2025–2028) funded by the Japan Society for the Promotion of Science, the Kato Foundation for Promotion of Science 2025 research grant, the Amano Institute of Technology 2024 research grant, and the Nippon Sheet Glass Foundation for Materials Science and Engineering 2025 research grant.

References

1 D. Dungworth: J. Archit. Conserv. **18** (2012) 7. https://doi.org/10.1080/13556207.2012.10785101
2 T. Kohli, M. Hubert, R. E. Youngman, and D. L. Morse: Int. J. Appl. Glass Sci. **13** (2022) 292. https://doi.org/10.1111/ijag.16560
3 Z. Sui, S. Qian, L. Niu, P. Hu, Z. Hua, X. Zheng, X. Sun, G. Tang, H. Cai, D. Yang, W. Li, M. Zhang, J. Han, and J. Ren: Innovation (Camb.) **6** (2025) 100878. https://doi.org/10.1016/j.xinn.2025.100878
4 T. Yanagida, T. Kato, D. Nakauchi, and N. Kawaguchi: Jpn. J. Appl. Phys. **62** (2022) 010508. https://doi.org/10.35848/1347-4065/ac9026
5 P. Lecoq: Nucl. Instrum. Methods Phys. Res. A **809** (2016) 130. https://doi.org/10.1016/j.nima.2015.08.041
6 T. Yanagida, A. Yoshikawa, Y. Yokota, K. Kamada, M. Ito, M. Takeda, N. Ohuchi, K. Uchiyama, and K. Mori: IEEE Trans. Nucl. Sci. **57** (2010) 1492. https://doi.org/10.1109/TNS.2009.2032265
7 J. Glodo, Y. Wang, R. Shawgo, C. Brecher, R. H. Hawrami, J. Tower, and K. S. Shah: Phys. Procedia **90** (2017) 285. https://doi.org/10.1016/j.phpro.2017.09.012
8 C. L. Melcher: Nucl. Instrum. Methods Phys. Res., Sect. B **40** (1989) 1214. https://doi.org/10.1016/0168-583X(89)90622-8
9 R. Mao, L. Zhang, and R.-Y. Zhu: IEEE Trans. Nucl. Sci. **55** (2008) 2425. https://doi.org/10.1109/TNS.2008.2000776
10 A. Antonelli, E. Auffray, S. Brovelli, F. Bruni, M. Campajola, S. Carsi, F. Carulli, G. De Nardo, E. Di Meco, E. Diociaiuti, A. Erroi, M. Francesconi, I. Frank, S. Kholodenko, N. Kratochwil, E. Leonardi, G. Lezzani, S. Mangiacavalli, S. Martellotti, M. Mirra, P. Monti-Guarnieri, M. Moulson, D. Paesani, E. Paoletti, L. Perna, P. Pierluigi, M. Prest, M. Romagnoni, A. Russo, I. Sarra, A. Selmi, F. Sgarbossa, M. Soldana, R. Tesauro, G. Tinti, and E. Vallazza: Nucl. Instrum. Methods Phys. Res. A **1069** (2024) 169877. https://doi.org/10.1016/j.nima.2024.169877
11 O. Sidletskiy, B. Grinyov, D. Kurtsev, I. Gerasymov, O. Zelenskaya, A. Baranov, J. Budagov, V. Glagolev, Y. Davydov, and V. Tarasov: Nucl. Instrum. Methods Phys. Res. A **735** (2014) 620. https://doi.org/10.1016/j.nima.2013.10.012

12 T. Yanagida, J. Ueda, H. Masai, Y. Fujimoto, and S. Tanabe: J. Non-Cryst. Solids. **431** (2016) 140. https://doi.org/10.1016/j.jnoncrysol.2015.04.033
13 H. Kimura, T. Fujiwara, M. Tanaka, T. Kato, D. Nakauchi, N. Kawaguchi, and T. Yanagida: J. Non-Cryst. Solids. **508** (2019) 46. https://doi.org/10.1016/j.jnoncrysol.2018.11.020
14 J. Fu, D. Bourdel, J. P. Bogard, P. Dufour, G. Raymond, and M. Fall: J. Non-Cryst. Solids. **326** (2003) 335. https://doi.org/10.1016/S0022-3093(03)00428-9
15 A. Nishikawa, D. Shiratori, T. Kato, D. Nakauchi, N. Kawaguchi, and T. Yanagida: Ceram. Int. **50** (2024) 3772. https://doi.org/10.1016/j.ceramint.2023.11.130
16 A. Khan, S. Saha, H. J. Kim, N. Wantana, J. Kaewkhao, S. Kothan, A. M. Abdalla, and H. B. Albargi: Radiat. Phys. Chem. **221** (2024) 111728. https://doi.org/10.1016/j.radphyschem.2024.111728
17 Y. Nakabayashi, Y. Fujimoto, M. Koshimizu, and K. Asai: Opt. Mater. **142** (2023) 114136. https://doi.org/10.1016/j.optmat.2023.114136
18 Y. Isokawa, Y. Nakayama, K. Kamada, S. Tanabe, and T. Yanagida: Opt. Mater. **90** (2019) 187. https://doi.org/10.1016/j.optmat.2019.02.046
19 K. Hashimoto, D. Shiratori, D. Nakauchi, T. Kato, N. Kawaguchi, and T. Yanagida: J. Ceram. Soc. Jpn. **128** (2020) 267. https://doi.org/10.2109/jcersj2.20014
20 K. Kagami, Y. Fujimoto, M. Koshimizu, D. Nakauchi, T. Kato, and K. Asai: J. Mater. Sci.: Mater. Electron. **31** (2020) 4488. https://doi.org/10.1007/s10854-020-02997-5
21 Y. Nakabayashi, Y. Fujimoto, M. Koshimizu, H. Kawamoto, and K. Asai: J. Mater. Sci.: Mater. Electron. **35** (2024) 575. https://doi.org/10.1007/s10854-024-12307-y
22 Y. Nakabayashi, Y. Fujimoto, M. Koshimizu, H. Kawamoto, and K. Asai: J. Lumin. **266** (2024) 120283. https://doi.org/10.1016/j.jlumin.2023.120283
23 M. Ciecińska, P. Goj, A. Stoch, and P. Stoch: J. Therm. Anal. Calorim. **139** (2020) 1763. https://doi.org/10.1007/s10973-019-08606-w
24 S. Kapoor, R. E. Youngman, L. Ma, N. Lönnroth, S. J. Rzoska, M. Bockowski, L. R. Jensen, and M. Bauchy: Front. Mater. **6** (2019) 63. https://doi.org/10.3389/fmats.2019.00063
25 K. Bartosiewicz, V. Babin, K. Kamada, A. Yoshikawa, and M. Nikl: J. Lumin. **166** (2015) 117. https://doi.org/10.1016/j.jlumin.2015.05.015
26 S. Saha, A. V. Ntarisa, N. D. Quang, N. T. Luan, P. Q. Vuong, H. J. Kim, N. Intachai, S. Kothan, and J. Kaewkhao: Radiation Phys. Chem. **199** (2022) 110285. https://doi.org/10.1016/j.radphyschem.2022.110285
27 M. Moszyński, M. Kapusta, M. Mayhugh, D. Wolski, and S. Flyckt: IEEE Trans. Nucl. Sci. **44** (1997) 1052. https://doi.org/10.1109/23.603803
28 L. M. Bollinger and G. E. Thomas: Rev. Sci. Instrum. **32** (1961) 1044. https://doi.org/10.1063/1.1717610
29 A. Sato, M. Koshimizu, Y. Fujimoto, S. Komatsuzaki, S. Kishimoto, and K. Asai: Mater. Chem. Front. **6** (2022) 1470. https://doi.org/10.1039/D2QM00187J
30 M. Grodzicka-Kobylka, J. Szczęśniak, M. Wojcik, K. Szczęsniak, P. Hoszowska, A. Dąbrowski, and M. Moszyński: Nucl. Instrum. Methods Phys. Res. A **1019** (2022) 165858. https://doi.org/10.1016/j.nima.2021.165858
31 Z. Hua, G. Tang, L. Zheng, T. Wu, H. Ban, H. Cai, J. Han, H. Liu, S. Qian, L. Qin, Q. Wei, S. Liu, J. Ren, X. Y. Sun, and Y. Zhu: Ceram. Int. **49** (2023) 18844. https://doi.org/10.1016/j.ceramint.2023.03.006
32 S. Maeng, S. H. Lee, S. J. Park, and W. C. Choi: Radiat. Phys. Chem. **199** (2022) 110325. https://doi.org/10.1016/j.radphyschem.2022.110325
33 K. S. Shah, J. Glodo, W. Higgins, E. V. D. van Loef, W. W. Moses, S. E. Derenzo, and M. J. Weber: IEEE Trans. Nucl. Sci. **52** (2005) 3157. https://doi.org/10.1109/TNS.2005.860155
34 Y. Fu, Z. Chen, Y. Sun, Z. Gao, S. Wang, Y. Liu, Y. Fan, Y. Yanwei, J. Wang, and J. Junhua: Radiat. Phys. Chem. **226** (2025) 112280. https://doi.org/10.1016/j.radphyschem.2024.112280
35 R. Rajaramakrishna, S. Kaewjaeng, J. Kaewkhao, and S. Kothan: Opt. Mater. **102** (2020) 109826. https://doi.org/10.1016/j.optmat.2020.109826
36 N. Wantana, Y. Ruangtaweep, E. Kaewnuam, S. Kothan, H. J. Kim, A. Prasatkhetragarn, and J. Kaewkhao: Radiat. Phys. Chem. **185** (2021) 109497. https://doi.org/10.1016/j.radphyschem.2021.109497
37 M. Fayaz, S. Ali, M. Yousaf, S. R. Khan, M. J. Uddin, and A. U. Khan: Ceram. Int. **49** (2023) 24690. https://doi.org/10.1016/j.ceramint.2023.04.127
38 X. Y. Sun, D. G. Jiang, Y. Z. Sun, X. Zhang, Q. L. Hu, Y. Huang, and Y. Tao: J. Am. Ceram. Soc. **97** (2014) 3388. https://doi.org/10.1111/jace.13296
39 K. Payungkulanan, M. Tungjai, N. Wantana, N. Chanthima, C. S. Sarumaha, P. Pakawanit, C. Phoovasawat, K. Kanjanaboos, K. Choodam, H. J. Kim, and J. Kaewkhao: Radiat. Phys. Chem. **224** (2024) 112023. https://doi.org/10.1016/j.radphyschem.2024.112023

40 P. Demchenko, I. Pashuk, A. Voloshinovskii, A. Gektin, A. Krasnikov, T. Shalapska, G. Stryganyuk, and S. Zazubovich: J. Phys. D: Appl. Phys. **46** (2013) 235103. https://doi.org/10.1088/0022-3727/46/23/235103
41 H. Suzuki, T. A. Tombrello, C. L. Melcher, W. W. Moses, A. M. Day, and A. J. van Loef: Nucl. Instrum. Methods Phys. Res. A **346** (1994) 510. https://doi.org/10.1016/0168-9002(94)90586-X
42 Y. Nakabayashi, Y. Fujimoto, M. Koshimizu, and K. Asai: J. Mater. Sci.: Mater. Electron. **33** (2022) 19846. https://doi.org/10.1007/s10854-022-08805-6
43 K. Shinozaki, Y. Kitagawa, G. Okada, D. Nakauchi, N. Kawaguchi, and T. Yanagida: J. Lumin. **276** (2024) 120859. https://doi.org/10.1016/j.jlumin.2024.120859
44 W. M. Yen: Phosphor Handbook, S. Shionoya and H. Yamamoto, Eds. (CRC Press, United States, 2007) 2nd ed., Chap. 2.
45 V. Babin, P. Boháček, A. Krasnikov, M. Nik l, L. Vasylechko, and S. Zazubovich: J. Lumin. **277** (2025) 120945. https://doi.org/10.1016/j.jlumin.2024.120945
46 P. Dorenbos: J. Mater. Chem. C **11** (2023) 8129. https://doi.org/10.1039/D2TC04439K
47 A. D. Sontakke, J. Ueda, and S. Tanabe: J. Non-Cryst. Solids **431** (2015) 150. https://doi.org/10.1016/j.jnoncrysol.2015.04.005
48 H. Masai, I. Pashuk, A. Voloshinovskii, A. Gektin, A. Krasnikov, T. Shalapska, G. Stryganyuk, and S. Zazubovich: J. Lumin. **195** (2018) 413. https://doi.org/10.1016/j.jlumin.2017.11.063
49 V. Dormenev, A. Amelina, E. Auffray, K.-T. Brinkmann, G. Dosovitskiy, F. Cova, A. Fedorov, S. Gundacker, D. Kazlou, M. Korjik, N. Kratochwil, V. Ladygin, V. Mechinsky, M. Moritz, S. Nargelas, R. W. Novotny, P. Orsich, M. Salomoni, Y. Talochka, G. Tamulaitis, A. Vaitkevicius, A. Vedda, and H. G. Zaunick: Nucl. Instrum. Methods Phys. Res. A **1015** (2021) 165762. https://doi.org/10.1016/j.nima.2021.165762
50 M. Dutta, J. M. Kalita, and G. Wary: J. Fluoresc. **35** (2025) 4399. https://doi.org/10.1007/s10895-024-03836-0
51 C. M. Combes, P. Dorenbos, C. W. E. van Eijk, K. W. Krämer, and H. U. Güdel: J. Lumin. **82** (1999) 299. https://doi.org/10.1016/S0022-2313(99)00047-2
52 P. Dorenbos: Physica Status Solidi (A) **202** (2005) 195. https://doi.org/10.1002/pssa.200460106
53 X. Lai, Y. Tian, Y. Wang, H. Inui, and G. Gao: Opt. Mater. **120** (2021) 111391. https://doi.org/10.1016/j.optmat.2021.111391
54 D. Shiratori, D. Nakauchi, T. Kato, N. Kawaguchi, and T. Yanagida: Sens. Mater. **32** (2020) 1365. https://doi.org/10.18494/SAM.2020.2740
55 S. Tavernier: Experimental Techniques in Nuclear and Particle Physics (Springer, Berlin Heidelberg, 2010) pp. 1–306. https://doi.org/10.1007/978-3-642-00829-0
56 C. Struebing, M. B. Beckert, J. H. Nadler, B. Kahn, B. Wagner, and Z. Kang: J. Am. Ceram. Soc. **101** (2018) 1116. https://doi.org/10.1111/jace.15273
57 W. Chewpraditkul, N. Pattanaboonmee, N. Yawai, W. Chewpraditkul, P. Lertloypanyachai, K. Sreebunpeng, M. Yoshino, L. Liu, and D. Chen: Opt. Mater. **98** (2019) 109468. https://doi.org/10.1016/j.optmat.2019.109468
58 H. Samizo, K. Shinozaki, T. Kato, G. Okada, N. Kawaguchi, H. Masai, and T. Yanagida: Opt. Mater. **90** (2019) 64. https://doi.org/10.1016/j.optmat.2019.01.035
59 A. Khan, S. Saha, H. J. Kim, N. Wantana, J. Kaewkhao, S. Kothan, A. M. Abdalla, and H. B. Albargi: Radiat. Phys. Chem. **221** (2024) 111728. https://doi.org/10.1016/j.radphyschem.2024.111728
60 W. Chewpraditkul, X. He, D. Chen, Y. Shen, Q. Sheng, B. Yu, M. Nikl, R. Kucerkova, A. Beitlerova, C. Wanarak, and A. Phunpueok: Phys. Status Solidi A **208** (2011) 2830. https://doi.org/10.1002/pssa.201127365